Breaking and restoration of rotational symmetry for irreducible tensor operators on the lattice

Bing-Nan Lu, Timo A. Lähde, Dean Lee, and Ulf-G. Meißner

Breaking and restoration of rotational symmetry for irreducible tensor operators on the lattice

Bing-Nan Lu,[1] Timo A. Lähde,[1] Dean Lee,[2] and Ulf-G. Meißner[3, 1, 4]

[1]*Institute for Advanced Simulation, Institut für Kernphysik, and Jülich Center for Hadron Physics, Forschungszentrum Jülich, D-52425 Jülich, Germany*
[2]*Department of Physics, North Carolina State University, Raleigh, North Carolina 27695, USA*
[3]*Helmholtz-Institut für Strahlen- und Kernphysik and Bethe Center for Theoretical Physics,*
Universität Bonn, D-53115 Bonn, Germany
[4]*JARA-High Performance Computing, Forschungszentrum Jülich, D-52425 Jülich, Germany*

We study the breaking of rotational symmetry on the lattice for irreducible tensor operators and practical methods for suppressing such breaking. We illustrate the features of the general problem using an α cluster model for ^{8}Be. We focus on the lowest states with non-zero angular momentum and examine the matrix elements of multipole moment operators. We show that reduced matrix elements are well reproduced by averaging over all possible orientations of the quantum state. This averaging is performed in terms of a sum of matrix elements weighted by the Clebsch-Gordan coefficients of each orientation. For our α cluster model, we find that the effects of rotational symmetry breaking can be largely eliminated for lattice spacings of $a \leq 1.7$ fm, and we expect similar improvement for lattice Monte Carlo calculations.

I. INTRODUCTION

In recent years, lattice Monte Carlo calculations have been widely applied to the study of nuclear structure [1–3]. In particular, chiral Effective Field Theory (chiral EFT) combined with lattice methods has been employed to study the spectrum and structure of light and medium-mass nuclei [4–8]. In such calculations, continuous space-time is discretized and compactified, which simplifies the numerical treatment of path integrals. The mesh points uniformly span a cubic box, and boundary conditions (such as periodic ones) are imposed in each dimension. In general, on the lattice the bound state state energies and wave functions deviate from their continuum infinite-volume counterparts due to discretization errors and finite-volume effects.

Much effort has already been devoted to the removal of lattice artifacts in field-theoretical calculations. For instance, the finite-volume energy shifts for two-body bound states [9–18] and for two-body resonances and scattering problems [19–23] have been studied in detail. There is also ongoing research to extend these results to bound states with more than two constituents [12, 13, 24–28]. The removal of artifacts due to non-zero lattice spacing is a more complicated issue. For chiral EFT, the lattice improvement program proposed by Symanzik *et al.* [29–31] provides a framework for the systematical reduction of discretization errors. Such a method has also been applied to Yang-Mills theories [29, 30], gauge field theories [31–34] including QCD [35]. Also, Dudek *et al.* [36] have proposed a method where the continuum spin of meson [37] and baryon [38, 39] excited states in lattice QCD can be reliably identified. Meanwhile, Davoudi *et al.* [40] have quantified the breaking and restoration of rotational invariance at both tree level and one-loop level by means of lattice operators smeared over a finite spatial region.

On the lattice, the rotational symmetry group is reduced to the finite group of cubic rotations, according to $SO(3) \rightarrow SO(3,Z)$. Several basic rules based on the argument of rotational invariance are therefore violated on the lattice. For instance, in the continuum and infinite-volume limits, quantum bound states with angular momentum J form a degenerate multiplet of $2J+1$ components, while on the lattice these energy levels split into subgroups corresponding to

different irreducible representations (*irreps*) of the cubic group [41–43]. The sizes of such energy splittings are dictated by the lattice spacing, the extent of the finite volume, and the boundary conditions.

In Ref. [44], the breaking of rotational symmetry on the lattice for bound state energies was studied within an α cluster model. It was shown that the calculated energy is minimized when the natural separation between particles is commensurate with the distance between lattice points along the preferred lattice directions associated with a given angular momentum state[1]. It was also shown that the multiplet-averaged energy is closer to the continuum limit than any single energy level. These results can be applied to future *ab initio* lattice studies of nuclear systems where α cluster structures are important.

Here, we extend the analysis of the binding energy in Ref. [44] to other observables of interest, such as nuclear radii, quadrupole moments, and transition probabilities. For instance, an anomalously large radius compared with the usual $\sim A^{1/3}$ scaling law is indicative of structure analogous to halo nuclei [45, 46], while the intrinsic quadrupole moment is related to the appearance of rotational bands observed in deformed nuclei [47].

For this purpose, we consider irreducible tensor operators sandwiched between pairs of bound-state wave functions. In the continuum limit, such expressions can be factorized and simplified according to the Wigner-Eckart theorem. Due to the lack of rotational symmetry on the lattice, such factorization is no longer possible and the analysis becomes more involved. Similarly, continuum selection rules for electromagnetic transitions are not exactly satisfied on the lattice, and hence transitions that are absolutely forbidden (in the continuum) by rotational symmetry arguments may assume non-vanishing amplitudes on the lattice. Our objective in such cases is to find appropriate corrections to these matrix elements, in order to minimize symmetry-breaking effects.

We shall now proceed to investigate anisotropic lattice artifacts in the matrix elements of irreducible tensor operators, and search for a practical method to restore full rotational symmetry. The details

---
[1] By commensurate, we mean equal to the length of a given lattice vector.

of the chosen interaction are not essential to our general analysis. We therefore work with the same α cluster model as was used in Ref. [44], where the α-α interaction is approximated by an Ali-Bodmer type potential adjusted to produce a bound ^{8}Be nucleus.

II. THEORETICAL FRAMEWORK

A. Alpha cluster Hamiltonian

Let $m_\alpha = 3727.0$ MeV denote the mass of the α particle, and $\mu = m_\alpha/2$ the reduced mass. Our starting point is the continuum Hamiltonian

$$H \equiv -\frac{\nabla^2}{2\mu} + V(r), \tag{1}$$

where $r = \sqrt{x^2 + y^2 + z^2}$ is the distance between the two α particles, $V \equiv V_N + V_C$ is the α-α potential, including nuclear and Coulomb contributions.

While our two-body potential is identical to that used in Ref. [44], we shall briefly review its functional form and parameters. For the nuclear part of the α-α interaction, we use an isotropic Ali-Bodmer-type potential,

$$V_N(r) \equiv V_0 \exp(-\eta_0^2 r^2) + V_1 \exp(-\eta_1^2 r^2), \tag{2}$$

where $V_0 = -216.0$ MeV, $V_1 = 354.0$ MeV, $\eta_0 = 0.436$ fm^{-1} and $\eta_1 = 0.529$ fm^{-1}, determined by fixing the S- and D-wave α-α scattering lengths to their experimental values. The Coulomb potential is given by

$$V_C(r) \equiv \frac{4e^2}{r} \operatorname{erf}\left(\frac{\sqrt{3}r}{2R_\alpha}\right), \tag{3}$$

where $R_\alpha = 1.44$ fm is the radius of the α particle, e is the fundamental unit of charge and "erf" denotes the error function.

We note that with the above parameters, the ^{8}Be nucleus is unbound. Since our objective is to study bound-state properties, we increase V_0 by 30%. With this adjustment, the ^{8}Be nucleus possesses a ground state at $E(0^+) = -10.8$ MeV and one excited state at $E(2^+) = -3.3$ MeV, measured relative to the α-α threshold.

On the lattice, the spatial vector $\boldsymbol{r}$ assumes discrete values, and thus we may express the Hamiltonian (1) in terms of a matrix. In a box of size L, we impose periodic boundary conditions on the wave functions, according to

$$\psi(\boldsymbol{r} + \boldsymbol{n}_i L) = \psi(\boldsymbol{r}), \tag{4}$$

where the $\boldsymbol{n}_i$ with $i = x, y, z$ are unit vectors along the three coordinate axes. The energy eigenvalues and wave functions of ^{8}Be can then be obtained by diagonalization of a Hamiltonian matrix of dimension $(L/a)^3 \times (L/a)^3$.

We express the kinetic energy term of the Hamiltonian (1) by means of a finite difference. For instance, in one dimension we have

$$f''(x) \approx c_0^{(N)} f(x) + \sum_{k=1}^{N} c_k^{(N)} [f(x+ka) + f(x-ka)], \tag{5}$$

where a is the lattice spacing and $c_k^{(N)}$ is a fixed set of coefficients. The formula of order N involves $2N + 1$ lattice points, and the truncation error is of $\mathcal{O}(a^{2N})$. The coefficients $c_k^{(N)}$ can be found for $N \leq 4$ in Ref. [44]. Here, we express the Laplace operator using the $N = 4$ formula. This choice removes most of the rotational symmetry breaking effects due to the kinetic energy operator.

B. Lattice wave functions

The continuum Hamiltonian (1) is invariant under spatial rotations. As a result, the bound states of H form angular momentum multiplets. Let us denote the bound-state wave functions by ϕ_{lm}, where the integer l is the angular momentum and the integer m its z-component, with $-l \leq m \leq l$. For systems with more than one bound state with the same value of l, additional radial quantum numbers are required. Such cases are not considered here. The angular dependence of these wave functions are given by the spherical harmonics Y_{lm}.

On the lattice, the multiplets of angular momentum l are split into *irreps* of the cubic rotational group $SO(3,Z)$. The splitting patterns of the multiplets for $l \leq 8$ were given in Ref. [44]. In order to specify the wave functions belonging to the same *irrep*, we define a quantum number k valid on the lattice through the relation

$$R_z\left(\frac{\pi}{2}\right) \equiv \exp\left(-i\frac{\pi}{2}k\right), \tag{6}$$

where $R_z(\pi/2)$ is a rotation around the z-axis by $\pi/2$. The integers k equal m modulo 4, and are non-degenerate for each *irrep* of $SO(3,Z)$. We label the wave function $\psi_{l\tau k}$ for any eigenstate according to l, k and the *irrep* τ it belongs to. If the angular momentum l contains more than one "branch" belonging to the same *irrep*, we distinguish them by adding primes to the names of the *irreps*. For instance, the notation "$\psi_{6T'_2 1}$" denotes the wave function with $l = 6$ and $k = 1$, which belongs to the second T_2 *irrep*. Note that the quantum number l is only approximate on the lattice, in the sense that a wave function labeled by l can have overlap with an infinite number of *irreps* of the rotational group carrying angular momenta other than l. Nevertheless, such mixing is suppressed by powers of the lattice spacing. In the continuum limit, the wave functions $\psi_{l\tau k}$ form a complete basis for the subspace of bound states, and the corresponding energies are degenerate for the same angular momentum l. In contrast, on the lattice the energies depend on both l and the *irrep* τ.

In the continuum limit, we can write down unitary transformations from the ϕ_{lm} basis to the $\psi_{l\tau k}$ basis and *vice versa*,

$$\phi_{lm} \equiv \sum_{\tau k} U_{lm\tau k} \psi_{l\tau k}, \tag{7}$$

$$\psi_{l\tau k} \equiv \sum_{m} U^{-1}_{l\tau km} \phi_{lm}, \tag{8}$$

see Ref. [48] for details. As an example, we show the case of $l = 2$. The wave functions ψ_{2E0} and ψ_{2E2} belong to *irrep* E, and $\psi_{2T_2 1}$, $\psi_{2T_2 2}$, and $\psi_{2T_2 3}$ to *irrep* T_2. Following Ref. [48], we find

$$\psi_{2E0} = \phi_{20}, \qquad \psi_{2T_2 1} = \phi_{21}, \qquad \psi_{2T_2 3} = \phi_{2\bar{1}},$$

$$\psi_{2E2} = \sqrt{\frac{1}{2}}(\phi_{22} + \phi_{2\bar{2}}) \qquad \psi_{2T_2 2} = -i\sqrt{\frac{1}{2}}(\phi_{22} - \phi_{2\bar{2}}), \tag{9}$$

where for notational convenience, we have used $\bar{m}$ to denote $-m$.

On the lattice, we can obtain the bound state wave functions $\psi_{l\tau k}$ by simultaneously diagonalizing the lattice Hamiltonian (or transfer matrix [1]) and $R_z(\pi/2)$. Since the full rotational symmetry is broken, the angular momentum l should be viewed as a label that describes the angular momentum multiplet obtained by dialing the lattice spacing continuously to zero. Nevertheless, we can use the unitary transformation in Eq. (7) to define the wave functions ϕ_{lm} at non-zero lattice spacing. We do this even though the wave functions ϕ_{lm} are in general not exact eigenstates of H when the lattice spacing is non-zero.

We use the notation φ_{lm} to denote the continuum limit ($a \to 0$) of the lattice wave functions ϕ_{lm}. For lattice observables we use parentheses, e.g. $(f|O|i)$, to denote lattice matrix elements computed by summation over lattice sites. For continuum observables we use brackets, e.g. $\langle f|O|i \rangle$, to denote matrix elements computed by integration over continuous space.

Let us now consider the bound-state wave functions for a zero angular momentum state ϕ_{00}, and for a general angular momentum state ϕ_{lm}. Then, the matrix element of the multipole operator $r^l Y_{lm}$ sandwiched between ϕ_{00} and ϕ_{lm},

$$C_m \equiv (\phi_{lm}|r^l Y_{lm}|\phi_{00}) = \sum_{\mathbf{n}} \phi_{lm}^*(\mathbf{n}a)|\mathbf{n}a|^l Y_{lm}(\hat{\mathbf{n}})\phi_{00}(\mathbf{n}a), \quad (10)$$

should be independent of m for $a \to 0$. When using Eq. (7), the requirement that C_m satisfy this constraint provides a convenient check that the phases of ϕ_{lm} and $\psi_{l\tau k}$ agree with standard conventions, as defined in Ref. [48].

C. Factorization of the matrix elements

Consider a pair of wave functions $\phi_{l_1 m_1}(\mathbf{r})$ and $\phi_{l_2 m_2}(\mathbf{r})$. On the one hand, the lattice matrix element of the multipole moment operator $r^{l'} Y_{lm}$ is

$$(l_1 m_1|r^{l'} Y_{lm}|l_2 m_2) = \sum_{\mathbf{n}} \phi_{l_1 m_1}^*(\mathbf{n}a)|\mathbf{n}a|^{l'} Y_{lm}(\hat{\mathbf{n}})\phi_{l_2 m_2}(\mathbf{n}a), \quad (11)$$

where the summation runs over all lattice sites. We consider independent integers l and l' in the multipole moment operator, in order to keep the radial and angular degrees of freedom independent. This makes our conclusions sufficiently general and applicable to all irreducible tensor operators. On the other hand, the continuum version of this multipole matrix element is

$$\langle l_1 m_1|r^{l'} Y_{lm}|l_2 m_2 \rangle = \int d^3\mathbf{r}\, \varphi_{l_1 m_1}^*(\mathbf{r})r^{l'} Y_{lm}(\Omega)\varphi_{l_2 m_2}(\mathbf{r}), \quad (12)$$

where $\varphi_{l_1 m_1}(\mathbf{r})$ and $\varphi_{l_2 m_2}(\mathbf{r})$ denote the wave functions in the continuum limit. Matrix elements of the form (12) occur frequently in the calculation of various nuclear observables, such as mean square radii, quadrupole moments, and transition probabilities. Here, we focus on lattice artifacts that produce differences between the numerical values of Eqs. (11) and (12) at a given lattice spacing a, and methods for removing them.

According to the Wigner-Eckart theorem, the matrix element (12) can be expressed as a product of two factors: Clebsch-Gordan (C-G)

coefficients and the "reduced" matrix element that encodes the dynamics of the problem at hand. This gives

$$\langle l_1 m_1|r^{l'} Y_{lm}|l_2 m_2 \rangle = \langle l_1|r^{l'}|l_2 \rangle Q_{l_2 m_2, lm}^{l_1 m_1}, \quad (13)$$

with

$$\langle l_1|r^{l'}|l_2 \rangle \equiv \int dr\, r^{l'+2} R_1^*(r)R_2(r), \quad (14)$$

$$Q_{l_2 m_2, lm}^{l_1 m_1} \equiv \int d\Omega\, Y_{l_1 m_1}^*(\Omega)Y_{lm}(\Omega)Y_{l_2 m_2}(\Omega), \quad (15)$$

where $R_1(r)$ and $R_2(r)$ denote the radial parts of the wave functions $\varphi_{l_1 m_1}(\mathbf{r})$ and $\varphi_{l_2 m_2}(\mathbf{r})$, respectively.

The radial integral in Eq. (14) represents the matrix element of the moment operator of order l', and is independent of the quantum numbers m, m_1 and m_2. Meanwhile, $Q_{l_2 m_2, lm}^{l_1 m_1}$ can be written as a product of C-G coefficients according to

$$Q_{l_2 m_2, lm}^{l_1 m_1} = \sqrt{\frac{(2l+1)(2l_2+1)}{4\pi(2l_1+1)}} C_{l_2 0, l0}^{l_1 0} C_{l_2 m_2, lm}^{l_1 m_1}, \quad (16)$$

such that all of the dependence on the quantum numbers m, m_1, m_2 and l is absorbed into $Q_{l_2 m_2, lm}^{l_1 m_1}$. In Table I, we list the $Q_{l_2 m_2, lm}^{l_1 m_1}$ with $l_1 = l_2 = 2$ and $0 \le l \le 4$. Others can be obtained from standard tables of C-G coefficients.

On the lattice, writing the wave functions as products of radial and angular components is precluded due to rotational symmetry breaking. However, the Wigner-Eckart theorem is still applicable to each *irrep* of the cubic group. As a result, the lattice matrix elements that belong to the same *irrep* are related by C-G coefficients of the cubic group, which can be straightforwardly computed using decompositions into spherical harmonics [48, 49]. For instance,

$$(2T_2 1|r^2 Y_{2E0}|2T_2 1) = -\sqrt{\frac{1}{3}}(2T_2 1|r^2 Y_{2E2}|2T_2 \bar{1}), \quad (17)$$

where

$$Y_{2E0} = Y_{20}, \quad Y_{2E2} = \sqrt{\frac{1}{2}}(Y_{22} + Y_{2\bar{2}}), \quad (18)$$

analogously to the relations in Eq. (9). The factor $-\sqrt{1/3}$ is independent of the lattice spacing, box size, and details of the potential.

We shall divide the lattice matrix elements (11) by $Q_{l_2 m_2, lm}^{l_1 m_1}$ as defined in Eq. (16) whenever such factors are non-zero, even though the factorization (13) is not exact on the lattice. We denote the resulting quantity (for $Q_{l_2 m_2, lm}^{l_1 m_1} \neq 0$)

$$(l_1 m_1\|r^{l'} Y_{lm}\|l_2 m_2) \equiv (l_1 m_1|r^{l'} Y_{lm}|l_2 m_2)/Q_{l_2 m_2, lm}^{l_1 m_1}, \quad (19)$$

by double vertical lines. Such reduced lattice matrix elements all converge to $\langle l_1|r^{l'}|l_2 \rangle$ as $a \to 0$. However, at non-zero lattice spacing the ratio will depend on the quantum numbers m, m_1, and m_2. The splittings between the components of Eq. (19) are therefore indicative of the rotational symmetry breaking effects.

l_1	l	l_2	m_1	m	m_2	$Q^{l_1 m_1}_{l_2 m_2, lm}$	m_1	m	m_2	$Q^{l_1 m_1}_{l_2 m_2, lm}$
2	0	2	0	0	0	$\frac{1}{2\sqrt{\pi}}$	1	0	1	$\frac{1}{2\sqrt{\pi}}$
			2	0	2	$\frac{1}{2\sqrt{\pi}}$				
2	2	2	0	0	0	$\frac{1}{7}\sqrt{\frac{5}{\pi}}$	2	1	1	$\sqrt{\frac{15}{14\pi}}$
			2	0	2	$-\frac{1}{7}\sqrt{\frac{5}{\pi}}$	1	1	0	$\frac{1}{14}\sqrt{\frac{5}{\pi}}$
			2	2	0	$-\frac{1}{7}\sqrt{\frac{5}{\pi}}$	1	0	1	$\frac{1}{14}\sqrt{\frac{5}{\pi}}$
			1	2	$\bar{1}$	$-\sqrt{\frac{15}{14\pi}}$				
2	4	2	0	0	0	$\frac{3}{7\sqrt{\pi}}$	1	3	$\bar{2}$	$\frac{1}{2}\sqrt{\frac{5}{7\pi}}$
			2	0	2	$\frac{1}{14\sqrt{\pi}}$	1	2	$\bar{1}$	$-\frac{1}{7}\sqrt{\frac{10}{\pi}}$
			2	1	1	$-\frac{1}{14}\sqrt{\frac{5}{\pi}}$	1	0	1	$-\frac{2}{7\sqrt{\pi}}$
			1	1	0	$\frac{1}{7}\sqrt{\frac{15}{2\pi}}$	2	2	0	$\frac{1}{14}\sqrt{\frac{15}{\pi}}$
			2	4	$\bar{2}$	$\sqrt{\frac{5}{14\pi}}$				

Table I. The factors $Q^{l_1 m_1}_{l_2 m_2, lm}$ defined in Eq. (16) with $l_1 = l_2 = 2$ and $0 \leq l \leq 4$. Those not given here can be obtained by means of standard tables of C-G coefficients.

D. Isotropic average

We shall now focus on the removal of spatial anisotropies associated with the orientation of the lattice wave functions relative to the lattice axes. We start with the continuum wave functions $\varphi_{l_1 m_1}$ and $\varphi_{l_2 m_2}$ and define the "skewed" matrix element

$$
\begin{aligned}
&\langle l_1 m_1 | r^{l'} Y_{lm} | l_2 m_2 \rangle_\Lambda \\
&\equiv \int d^3 \boldsymbol{r}\, \varphi^*_{l_1 m_1}(R(\Lambda)\boldsymbol{r})\, r^{l'} Y_{lm}(R(\Lambda)\Omega)\, \varphi_{l_2 m_2}(R(\Lambda)\boldsymbol{r}),
\end{aligned} \quad (20)
$$

where $\Lambda \equiv (\alpha, \beta, \gamma)$ is a set of Euler angles and $R(\Lambda)$ is an element of the $SO(3)$ rotation group. We also define the isotropically averaged matrix element

$$
\begin{aligned}
\langle l_1 m_1 | r^{l'} Y_{lm} | l_2 m_2 \rangle_\circ &\equiv \int d^3 \Lambda\, \langle l_1 m_1 | r^{l'} Y_{lm} | l_2 m_2 \rangle_\Lambda \\
&= C^{l_1 m_1}_{l_2 m_2, lm} \left[\frac{1}{2l_1+1} \sum_{m', m'_1, m'_2} C^{l_1 m'_1}_{l_2 m'_2, lm'} \langle l_1 m'_1 | r^{l'} Y_{lm'} | l_2 m'_2 \rangle \right],
\end{aligned} \quad (21)
$$

where $d^3 \Lambda$ is the normalized invariant measure on the $SO(3)$ group space and the subscript "$\circ$" denotes the isotropic average. We note that rotational invariance of the integral measure guarantees that $\langle l_1 m_1 | r^{l'} Y_{lm} | l_2 m_2 \rangle$, $\langle l_1 m_1 | r^{l'} Y_{lm} | l_2 m_2 \rangle_\Lambda$, and $\langle l_1 m_1 | r^{l'} Y_{lm} | l_2 m_2 \rangle_\circ$ are all equal. What is particularly useful is that the last expression in Eq. (21) encodes the process of angular averaging in terms of C-G coefficients, and can be applied to lattice matrix elements. We shall use this to remove anisotropies associated with the orientation of the lattice axes.

Following Eq. (21), we define the isotropically averaged lattice matrix element

$$
(l_1 m_1 | r^{l'} Y_{lm} | l_2 m_2)_\circ
$$

$$
\equiv C^{l_1 m_1}_{l_2 m_2, lm} \left[\frac{1}{2l_1+1} \sum_{m', m'_1, m'_2} C^{l_1 m'_1}_{l_2 m'_2, lm'} (l_1 m'_1 | r^{l'} Y_{lm'} | l_2 m'_2) \right], \quad (22)
$$

where it is again convenient to define an isotropically averaged reduced matrix element according to

$$
(l_1 \| r^{l'} Y_l \| l_2)_\circ \equiv (l_1 m_1 | r^{l'} Y_{lm} | l_2 m_2)_\circ / Q^{l_1 m_1}_{l_2 m_2, lm} \quad (23)
$$

for $Q^{l_1 m_1}_{l_2 m_2, lm} \neq 0$. For $a \to 0$, $(l_1 \| r^{l'} Y_l \| l_2)_\circ$ coincides with the radial matrix element $\langle l_1 | r^{l'} | l_2 \rangle$.

We note that the radial matrix element $\langle l_1 | r^{l'} | l_2 \rangle$ is not only independent of m, m_1 and m_2, but also independent of l. So, a non-trivial test of rotational symmetry restoration is to check that $(l_1 \| r^{l'} Y_l \| l_2)_\circ$ as defined in Eq. (23) is independent of l. If $(l_1 \| r^{l'} Y_l \| l_2)_\circ$ is to a good approximation independent of l, then we have succeeded in (approximately) factorizing the radial and angular parts of the lattice wave function by means of isotropic averaging. We will test this numerically with the α cluster model in Sec. III.

III. RESULTS

We first consider the mean square radius operator r^2. This corresponds to setting $l = 0$ and $l' = 2$ in Eqs. (11) and (12). In the upper panel of Fig. 1, we show the expectation values of r^2 for the lowest 2^+ states as functions of the lattice spacing a. The eigenstate wave functions $\psi_{2\tau k}$ are obtained by simultaneous diagonalization of the lattice Hamiltonian and the $R_z(\pi/2)$ operator. We then construct the linear combinations ϕ_{2m} according to Eq. (9). We use $(m\|0\|m)$ as an abbreviation for $(2m\|r^2 Y_{00}\|2m)$, and the solid curve denotes the isotropic average $(2\|r^2 Y_{00}\|2)_\circ$ defined in Eq. (23). Only three values with $m \geq 0$ are shown, since time reversal symmetry ensures equal results for m and $-m$. As discussed in Sec. II, all these reduced matrix elements converge to $\langle r^2 \rangle \equiv \langle l_1 = 2 | r^2 | l_2 = 2 \rangle$ in the limit $a \to 0$. Note that in all the following calculations, we suppress the finite volume effects by means of a large box of size $L \geq 16$ fm.

The three branches in Fig. 1 are not linearly independent because of the cubic symmetries on the lattice. For scalar operators, the linear relations among them are manifest. According to Eq. (9), the wave functions ϕ_{21} and ϕ_{20} belong to *irreps* E and T_2, respectively. Similarly, the wave function ϕ_{22} is a mixture of the *irreps* E and T_2 with equal weights. Thus $(2\|0\|2)$ equals the arithmetic average of $(0\|0\|0)$ from *irrep* E and $(1\|0\|1)$ from *irrep* T_2. So, we find that the isotropically averaged reduced matrix element $(2\|r^2 Y_0\|2)_\circ$ is given by

$$
(2\|r^2 Y_0\|2)_\circ = \frac{3}{5}(1\|0\|1) + \frac{2}{5}(0\|0\|0), \quad (24)
$$

where the factors 3 and 2 in the numerators are simply the dimensionalities of the cubic representations. It is easy to verify that the weighted average formula is applicable for any angular momentum, provided that the factors 3 and 2 in Eq. (24) are replaced by the corresponding *irrep* dimensionalities. In Ref. [44], we introduced the multiplet-weighted average to eliminate the anisotropic effects in the bound-state energies. We have now shown that this procedure is equivalent to averaging over lattice orientations and applies to the expectation value of any scalar operator.

Next, let us examine the dependence of these reduced matrix elements on the lattice spacing a. For $a \leq 1.0$ fm, the three branches in Fig. 1 merge, and for large a they split and exhibit oscillations. Before discussing the physics behind these observations, it is interesting to compare Fig. 1 in this paper to Fig. 3 in Ref. [44], where the calculated energies of the 2^+ states are shown as a function of a. We immediately find that these figures are similar if we map $(1\|0\|1)$ to $E(2_T^+)$, and $(0\|0\|0)$ to $E(2_E^+)$. Specifically, in Fig. 1 the splitting between the two branches vanishes at $a \simeq 1.4$ fm and $\simeq 1.9$ fm. For $a \leq 1.0$ fm, the splitting is negligible. For $1.0 \leq a \leq 1.4$ fm, $(1\|0\|1)$ is higher than $(0\|0\|0)$. In the region $1.4 \leq a \leq 1.9$ fm, the situation is reversed. For $a \geq 1.9$ fm, $(1\|0\|1)$ is once again higher and the splitting increases monotonically. Such behavior also occurs for the energies in Ref. [44] with slightly different turning points. Additionally, the weighted averages $(2\|r^2 Y_0\|2)_\circ$ and $E(2_A^+)$ both show "down bending" in the transitional region $1.5 \leq a \leq 2.0$ fm, resulting in smaller expectation values for both energy and radii at large lattice spacings.

Similar behavior as a function of a is found for other scalar operators. In the lower panel of Fig. 1, we show results for the r^4 operator, which correspond to setting $l = 0$ and $l' = 4$. Here, $(m\|0\|m)$ is an abbreviation of $(2m\|r^4 Y_{00}\|2m)$ and the solid curve denotes the isotropic average. All the curves converge to the expectation value $\langle r^4 \rangle \equiv \langle l_1 = 2|r^4|l_2 = 2 \rangle$ as $a \to 0$. Again, the isotropic average equals the multiplet-weighted average over the five-fold multiplet ϕ_{2m}. The oscillations of these components as well as the "down bending" of the isotropic average are similar to those observed for the r^2 operator.

As noted in Ref. [44] for the binding energies, these oscillations are associated with the commensurability of the lattice with the size and shape of the lattice wave functions. The lattice wave functions receive large contributions from lattice vectors which form the corresponding representation of the cubic rotational group and are closest in length to the (continuum limit) average separation distance R between constituent particles. Roughly speaking, if the lattice vectors closest in length to R are shorter than R, then $\langle r^2 \rangle$ and $\langle r^4 \rangle$ fall below the continuum value. Conversely, if the lattice separation vectors closest in length to R are longer than R, then $\langle r^2 \rangle$ and $\langle r^4 \rangle$ will exceed the continuum value. Although we find that isotropic averaging removes most of these oscillations, some remnants of this oscillatory behavior remain in the isotropically-averaged results.

Given the results shown in Fig. 1, we can compare the components $(m\|0\|m)$ to the continuum limit and determine which ones exhibit the least dependence on a. On the one hand, we find that $(1\|0\|1)$ and $(0\|0\|0)$ are not particularly reliable estimators for $\langle r^2 \rangle$ and $\langle r^4 \rangle$ on coarse lattices. On the other hand, the arithmetic average $(2\|0\|2)$ and the multiplet-weighted average both provide a good description of the continuum values over a wide range of lattice spacings. In principle, both could be used as a good approximation to the continuum limit. The multiplet-weighted average is theoretically preferable because of its clear physical interpretation as isotropic averaging. Our conclusions for the operators r^2, r^4 as well as the energy apply straightforwardly to other scalar operators on the lattice. For instance, the linear relation among the components $(0\|0\|0)$, $(1\|0\|1)$ and $(2\|0\|2)$ remains satisfied. To estimate the continuum expectation values, we evaluate the isotropic average according to Eq. (23). For scalar operators, this equals the weighted average over the angular momentum multiplet.

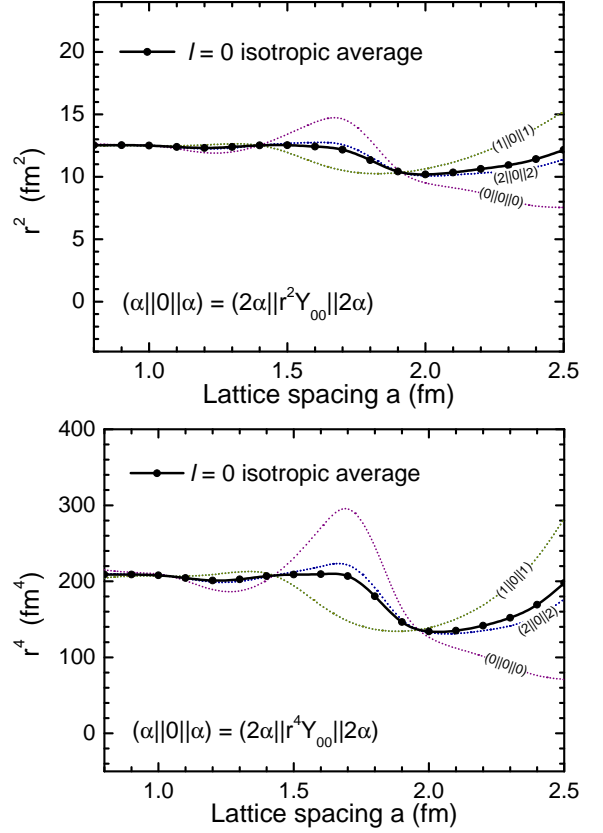We now turn to the case of $l = 2$. In the upper panel of Fig. 2,

Figure 1. (color online). *Upper panel*: Mean square radii $\langle r^2 \rangle$ for the lowest 2^+ states of the ^{8}Be nucleus as a function of a. $(\alpha\|0\|\alpha)$ is an abbreviation of $(2\alpha\|r^2 Y_{00}\|2\alpha)$, as defined in Eq. (19). The box size $L > 16$ fm suppresses finite-volume effects. The solid line gives the isotropic average $(2\|r^2 Y_0\|2)_\circ$ according to Eq. (23). *Lower panel*: Mean value $\langle r^4 \rangle$ for the lowest 2^+ states of the ^{8}Be nucleus as a function of a. $(\alpha\|0\|\alpha)$ is an abbreviation of $(2\alpha\|r^4 Y_{00}\|2\alpha)$, and the solid line gives the isotropic average $(2\|r^4 Y_0\|2)_\circ$.

the $(\alpha\|\beta\|\gamma)$ are abbreviations of the reduced matrix elements $(2\alpha\|r^2 Y_{2\beta}\|2\gamma)$ defined in Eq. (19), where the subscripts α, β and γ run from -2 to 2 and only the components with $\alpha = \beta + \gamma$ are shown. The solid curve represents the isotropic average defined in Eq. (23). All these curves converge to the expectation value $\langle r^2 \rangle$ as $a \to 0$. As the $2l + 1$ wave functions in an angular momentum multiplet mix on the lattice, some components with $\alpha \neq \beta + \gamma$ survive for large lattice spacings. However, because the corresponding C-G coefficients vanish in this case, such components do not contribute to the isotropic average.

Compared to the case of the scalar operator r^2 shown in Fig. 1, the insertion of the spherical harmonic $Y_{2\beta}$ makes the situation much more complicated, as shown in Fig. 2. Still, we can draw some general conclusions. First, as for the scalar operators, we can show that $(2\|0\|2)$ equals the arithmetic average of $(1\|0\|1)$ and $(0\|0\|0)$, while $(2\|2\|0)$ equals that of $(1\|1\|0)$ and $(0\|0\|0)$. This point is apparent in Fig. 2, if we note that in each group the three curves intersect at a single point. Second, applying the Wigner-Eckart theorem for the cubic group, we obtain multiple linear identities between the lattice matrix elements. These involve not only the components shown in Fig. 2, but also those that vanish as $a \to 0$.
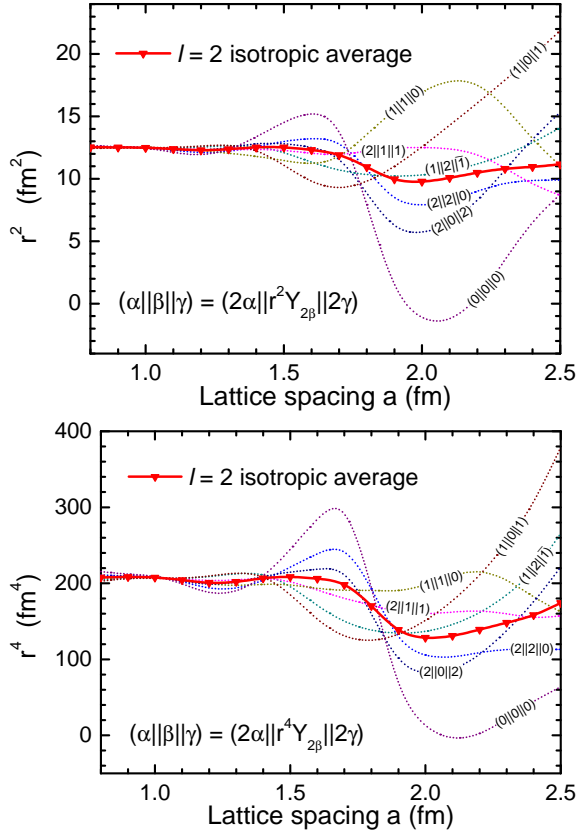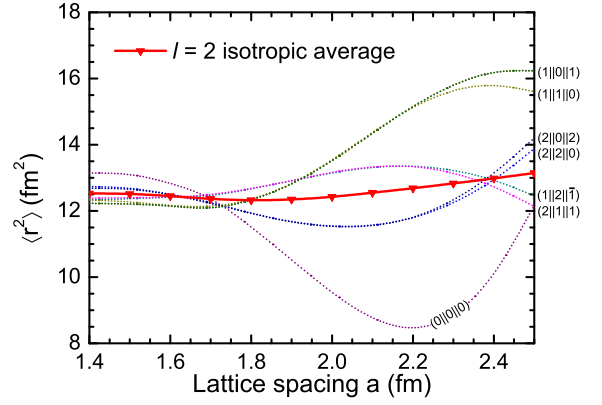
Figure 3. (color online) Mean square radii $\langle r^2 \rangle$ calculated with wave functions for $a/2$. This effectively factorizes out discretization errors due to the wave functions. The solid line represents the isotropic average $(2\|r^2Y_2\|2)_\circ$ defined in Eq. (23). Only results with large a are shown due to box size limitations. Note that the residual splittings for small a are a result of the finite-volume effects.

Figure 2. (color online). *Upper panel*: Mean square radii $\langle r^2 \rangle$ for the lowest 2^+ states of the ^{8}Be nucleus as a function of a. $(\alpha\|\beta\|\gamma)$ is an abbreviation of $(2\alpha\|r^2Y_{2\beta}\|2\gamma)$, as defined in Eq. (19). The solid line gives the isotropic average $(2\|r^2Y_2\|2)_\circ$ according to Eq. (23). *Lower panel*: Mean value $\langle r^4 \rangle$ for the lowest 2^+ states of the ^{8}Be nucleus as a function of a. $(\alpha\|\beta\|\gamma)$ is an abbreviation of $(2\alpha\|r^4Y_{2\beta}\|2\gamma)$, and the solid line gives the isotropic average $(2\|r^4Y_2\|2)_\circ$.

In the upper panel of Fig. 2, most of the components oscillate and exhibit more than one extremum in this region. For instance, $(0\|0\|0)$ reaches a maximum at $a = 1.6$ fm and possesses two minima at $a = 1.2$ fm and 2.1 fm, respectively. In contrast, $(1\|0\|1)$ has only one minimum at $a = 1.8$ fm. For large lattice spacings, the individual components deviate from the continuum values by as much as $\sim 100\%$. Interestingly, an "anomaly" occurs at $a = 2.1$ fm, where the matrix element $(0\|0\|0)$ becomes negative, whereas the expectation value $\langle r^2 \rangle$ is positive in the continuum limit. This discrepancy arises because we do not calculate $\langle r^2 \rangle$ with the same wave functions on both sides, as was the case for scalar operators in Fig. 1. For the $l = 2$ matrix elements in Fig. 2, the reduced matrix element $(0\|0\|0)$ is defined to be proportional to the expectation value of the quadrupole operator r^2Y_{20}. On the lattice, the angular part of the quadrupole operator cannot be completely separated, and thus the insertion of the spherical harmonic Y_{20} is not fully canceled by the C-G coefficients included in Eq. (19). We find that the resulting lattice artifacts may become as large as the magnitude of the observable itself. This suggests that random selection of matrix elements on coarse lattices with $a \simeq 2$ fm leads to inherently unrealistic results.

In spite of the large differences between the components $(\alpha\|\beta\|\gamma)$

on coarse lattices, we find that the anisotropy of the lattice artifacts can be eliminated by means of the isotropic average defined in Eq. (23). In the upper panel of Fig. 2, the isotropic average is given by the solid line. Note that the isotropic average can no longer be written as a multiplet-weighted average, as the C-G coefficients are no longer identical. As for the isotropic average shown in the upper panel of Fig. 1, the isotropic average in Fig. 2 bends slightly downward in the region 1.5 fm $\leq a \leq$ 2.0 fm. For the lattice spacings considered here, the range of values obtained are between 9.8 fm^2 and 12.5 fm^2, accounting for no more than a $\sim 20\%$ relative error with respect to the continuum limit.

On the lattice, the angular parts of the wave functions deviate from the spherical harmonics. We shall briefly study how much of the observed discretization errors are due to such distortion of the wave functions. For this purpose, we may consider the isotropic average using wave functions with greatly reduced lattice artifacts. In Fig. 3, we show results similar to the upper panel of Fig. 2, with the exception that the wave functions more closely resemble those of the continuum limit. Specifically, for each value of the lattice spacing a, we calculate the wave functions by diagonalizing the lattice Hamiltonian for $a/2$, after which matrix elements are computed with the original lattice spacing a. For instance, given $a = 2.5$ fm, we use the wave functions obtained with $a = 1.25$ fm, while dropping all mesh points that are absent for $a = 2.5$ fm. This has the effect of minimizing distortion due to the wave functions, such that the remaining effects are due to the discrete summation. We find that the splittings for large a are much smaller than in Fig. 2, indicating that effects due to the wave functions are largely responsible for the observed lattice artifacts. Furthermore, the isotropic average reproduces the continuum values very well and the "down bending" in Fig. 2 no longer appears.

Now, let us vary the radial factor of the inserted operator and keep the angular part the same. In the lower panel of Fig. 2, $(\alpha\|\beta\|\gamma)$ denotes the reduced lattice matrix element $(2\alpha\|r^4Y_{2\beta}\|2\gamma)$ which converges to $\langle r^4 \rangle$ as $a \to 0$. The solid line represents the isotropic average $(2\|r^4Y_2\|2)_\circ$. Again, the spherical harmonic $Y_{2\beta}$ is not fully canceled by the C-G coefficients on the lattice. For large lattice spac-
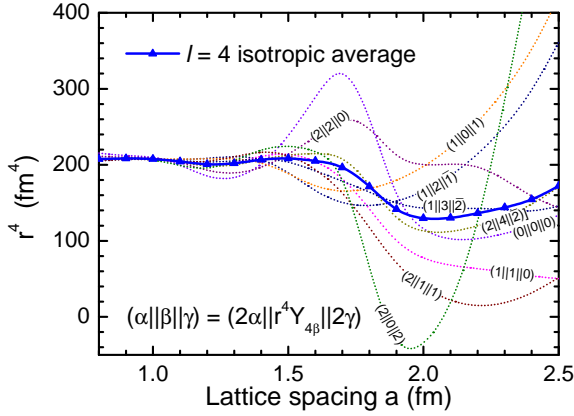
Figure 4. (color online) Mean value $\langle r^4 \rangle$ for the lowest 2^+ states of the ^{8}Be nucleus as a function of a. $(\alpha\|\beta\|\gamma)$ is an abbreviation of $(2\alpha\|r^4Y_{4\beta}\|2\gamma)$, as defined in Eq. (19). The solid line gives the isotropic average $(2\|r^4Y_4\|2)_\circ$ according to Eq. (23).

ings, the resulting lattice artifacts shift the various components from the continuum limit by differing amounts. Nevertheless, comparing the curves denoted by the same symbol in the upper and lower panel of Fig. 2, we find that their behavior is *qualitatively* similar. For example, the $(0\|0\|0)$ curves both show a maximum at $a = 1.6$ fm and a minimum at $a = 2.1$ fm, while the $(2\|0\|2)$ curves both show a minimum at $a = 2.0$ fm. In other words, the magnitude of the lattice artifacts may be different if the radial part of the inserted operator is changed, but the pattern of deviations is largely determined by the angular momenta of the states and the irreducible tensor operator.

We also consider irreducible tensor operators with $l = 4$. In Fig. 4, $(\alpha\|\beta\|\gamma)$ denotes the reduced lattice matrix element $(2\alpha\|r^4Y_{4\beta}\|2\gamma)$, which converges to $\langle r^4 \rangle$ as $a \to 0$. The solid line gives the isotropic average $(2\|r^4Y_4\|2)_\circ$. The number of independent components is now larger than for $l = 2$, which leads to qualitatively different behavior. For instance, $(0\|0\|0)$ is much closer to the isotropic average compared to the corresponding curve in the lower panel of Fig. 2. Also, the $(2\|0\|2)$ curve now exhibits a pronounced minimum at $a = 2.0$ fm.

Let us finally study to what extent anisotropies due to lattice artifacts are removed by isotropic averaging according to Eq. (23). In the upper panel of Fig. 5, we show a comparison between the isotropic averages $(2\|r^2Y_0\|2)_\circ$ and $(2\|r^2Y_2\|2)_\circ$. The former is calculated by a simple multiplet averaging over the five-fold branches, while the latter is obtained by a more complicated averaging with the C-G coefficients as weights. Clearly, for all lattice spacings considered here, the difference between the two curves is rather small. Especially, the "down bending" occurs for the same lattice spacing and the magnitudes of the deviations are also similar. Given that the C-G coefficients are included explicitly in the definition of isotropic average (23), we conclude that the effect of the angular part of the inserted operators is canceled by the C-G coefficients in the denominator. As discussed in Section II, this provides strong evidence for approximate rotational symmetry restoration, and that we have effectively succeeded in factorizing the radial and angular parts of the lattice wave function.

In the lower panel of Fig. 5, we show the quantities that converge to $\langle r^4 \rangle$ as $a \to 0$, including $(2\|r^4Y_0\|2)_\circ$, $(2\|r^4Y_2\|2)_\circ$ and
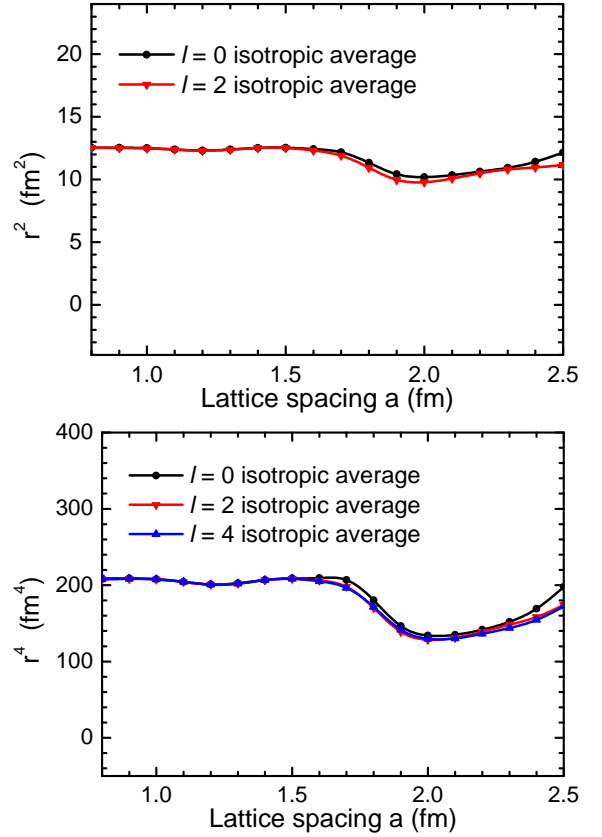

Figure 5. (Color online) *Upper panel*: Mean square radii $\langle r^2 \rangle$ for the lowest 2^+ states of the ^{8}Be nucleus as a function of a. The black and red lines represent the isotropic average $(2\|r^2Y_0\|2)_\circ$ and $(2\|r^2Y_2\|2)_\circ$, respectively. *Lower panel*: Expectation value $\langle r^4 \rangle$ for the lowest 2^+ states of the ^{8}Be nucleus as a function of a. The black, red and blue lines represent the isotropic averages $(2\|r^4Y_0\|2)_\circ$, $(2\|r^4Y_2\|2)_\circ$, and $(2\|r^4Y_4\|2)_\circ$, respectively.

$(2\|r^4Y_4\|2)_\circ$. The three curves coincide even for $a > 2.0$ fm, which indicates that rotational symmetry is restored to a large extent after isotropic averaging. In particular, the difference between the $l = 2$ and $l = 4$ results is negligible for all lattice spacings.

IV. CONCLUSIONS

In summary, we have studied the breaking of rotational symmetry due to lattice artifacts, with emphasis on how the degeneracy of multiplets of bound states with the same angular momentum is affected. On the lattice, the bound-state wave functions are classified according to the irreducible representations of the cubic group instead of the full $SO(3)$ rotational group. This leads to significant complications in the treatment of observables represented by irreducible tensor operators. Here, we have used an α cluster model to study the lattice matrix elements of such operators, and found that the qualitative behavior of the various matrix elements as a function of lattice spacing is mainly determined by the angular momentum quantum numbers of the states and operators. The matrix elements of different operators with the same angular momentum show similar behavior as a function of the lattice spacing.

In order to minimize the effects of rotational symmetry break-

ing, we have introduced an "isotropic average", which consists of a linear combination of the components of the matrix element. The weight of a given component is given by the C-G coefficient with the associated quantum numbers. We have shown that this method is equivalent to averaging over all possible lattice orientations. We have also found that isotropic averaging eliminates, to a good approximation, the anisotropy caused by lattice artifacts. This is illustrated by numerical calculations for the ^{8}Be nucleus within the α cluster model.

We have considered the isotropic averages of several irreducible tensor operators for different angular momenta, and studied their dependence on the lattice spacing. In all cases, we found excellent agreement with the continuum values. As a function of lattice spacing, the isotropically averaged $\langle r^2 \rangle$ and $\langle r^4 \rangle$ slightly underestimate the continuum values in the region 1.7 fm $\leq a \leq 2.0$ fm. For $a < 1.7$ fm, the deviation from the continuum is very small. As noted in Ref. [44], some rotational symmetry breaking effects arise from the commensurability of the underlying lattice with the magnitude and shape of the bound-state wave function. With isotropic averaging, we are in essence evening out such differences by averaging over all possible orientations of the lattice axes. While this does not remove all lattice artifacts, the dependence on the lattice spacing is substantially reduced.

While the present conclusions were obtained within a simple α cluster model, the method of isotropic averaging is immediately applicable to *ab initio* lattice Monte Carlo results. For instance, in the lattice calculation of transition amplitudes between low-energy excited states and the ground state of a nucleus, our method is expected to provide an immediate improvement by removing unphysical level splittings and minimizing the dependence on the lattice spacing.

[1] D. Lee, Prog. Part. Nucl. Phys. **63**, 117 (2009).

[2] A. Bazavov, D. Toussaint, C. Bernard, J. Laiho, C. DeTar, L. Levkova, M. B. Oktay, S. Gottlieb, U. M. Heller, J. E. Hetrick, P. B. Mackenzie, R. Sugar, and R. S. Van de Water, Rev. Mod. Phys. **82**, 1349 (2010).

[3] S. Beane, W. Detmold, K. Orginos, and M. Savage, Prog. Part. Nucl. Phys. **66**, 1 (2011).

[4] B. Borasoy, E. Epelbaum, H. Krebs, D. Lee, and U.-G. Meißner, Eur. Phys. J. A **31**, 105 (2007).

[5] E. Epelbaum, H. Krebs, D. Lee, and U.-G. Meißner, Eur. Phys. J. A **45**, 335 (2010).

[6] E. Epelbaum, H. Krebs, D. Lee, and U.-G. Meißner, Phys. Rev. Lett. **104**, 142501 (2010).

[7] E. Epelbaum, H. Krebs, D. Lee, and U.-G. Meißner, Phys. Rev. Lett. **106**, 192501 (2011).

[8] E. Epelbaum, H. Krebs, T. A. Lähde, D. Lee, and U.-G. Meißner, Phys. Rev. Lett. **110**, 112502 (2013).

[9] M. Lüscher, Comm. Math. Phys. **104**, 177 (1986).

[10] M. Lüscher, Nucl. Phys. B **354**, 531 (1991).

[11] S. Beane, P. Bedaque, A. Parreño, and M. Savage, Phys. Lett. B **585**, 106 (2004).

[12] S. König, D. Lee, and H.-W. Hammer, Phys. Rev. Lett. **107**, 112001 (2011).

[13] S. König, D. Lee, and H.-W. Hammer, Annals Phys. **327**, 1450 (2012), arXiv:1109.4577 [hep-lat].

[14] S. Bour, S. König, D. Lee, H.-W. Hammer, and U.-G. Meißner, Phys. Rev. **84**, 091503 (2011), arXiv:1107.1272 [nucl-th].

[15] Z. Davoudi and M. J. Savage, Phys. Rev. D **84**, 114502 (2011).

[16] R. A. Briceño, Z. Davoudi, T. C. Luu, and M. J. Savage, arXiv:1311.7686 [hep-lat].

[17] R. A. Briceño, Z. Davoudi, T. C. Luu, and M. J. Savage, Phys. Rev. D **88**, 114507 (2013).

[18] D. Agadjanov, U.-G. Meißner, and A. Rusetsky, JHEP **01**, 103 (2014).

[19] V. Bernard, M. Lage, U.-G. Meißner, and A. Rusetsky, JHEP **08**, 024 (2008).

[20] M. Lage, U.-G. Meißner, and A. Rusetsky, Phys. Lett. B **681**, 439 (2009).

[21] V. Bernard, M. Lage, U.-G. Meißner, and A. Rusetsky, JHEP **01**, 019 (2011).

[22] M. Göckeler, R. Horsley, M. Lage, U.-G. Meißner, P. E. L. Rakow, A. Rusetsky, G. Schierholz, and J. M. Zanotti, Phys. Rev. D **86**, 094513 (2012).

[23] N. Li and C. Liu, Phys. Rev. D **87**, 014502 (2013).

[24] S. Kreuzer and H.-W. Hammer, Eur. Phys. J. A **43**, 229 (2010).

[25] S. Kreuzer and H.-W. Hammer, Phys. Lett. B **694**, 424 (2011).

[26] K. Polejaeva and A. Rusetsky, Eur. Phys. J. A **48**, 1 (2012).

[27] R. A. Briceño and Z. Davoudi, Phys. Rev. D **87**, 094507 (2013).

[28] U.-G. Meißner, G. Ríos, and A. Rusetsky, Phys. Rev. Lett. **114**, 091602 (2015).

[29] P. Weisz, Nucl. Phys. B **212**, 1 (1983).

[30] P. Weisz and R. Wohlert, Nucl. Phys. B **236**, 397 (1984).

[31] M. Lüscher and P. Weisz, Nucl. Phys. B **240**, 349 (1984).

[32] G. Curci, P. Menotti, and G. Paffuti, Phys. Lett. B **130**, 205 (1983).

[33] H. W. Hamber and C. M. Wucur, Phys. Lett. B **133**, 351 (1983).

[34] T. Eguchi and N. Kawamoto, Nucl. Phys. B **237**, 609 (1984).

[35] B. Sheikholeslami and R. Wohlert, Nucl. Phys. B **259**, 572 (1985).

[36] J. J. Dudek, R. G. Edwards, M. J. Peardon, D. G. Richards, and C. E. Thomas (for the Hadron Spectrum Collaboration), Phys. Rev. Lett. **103**, 262001 (2009).

[37] J. J. Dudek, R. G. Edwards, M. J. Peardon, D. G. Richards, and C. E. Thomas (for the Hadron Spectrum Collaboration), Phys. Rev. D **82**, 034508 (2010).

[38] R. G. Edwards, J. J. Dudek, D. G. Richards, and S. J. Wallace, Phys. Rev. D **84**, 074508 (2011).

[39] S. Meinel, Phys. Rev. D **85**, 114510 (2012).

[40] Z. Davoudi and M. J. Savage, Phys. Rev. D **86**, 054505 (2012).

[41] R. Johnson, Phys. Lett. B **114**, 147 (1982).

[42] B. Berg and A. Billoire, Nucl. Phys. B **221**, 109 (1983).

[43] J. E. Mandula, G. Zweig, and J. Govaerts, Nucl. Phys. B **228**, 91 (1983).

[44] B.-N. Lu, T. A. Lähde, D. Lee, and U.-G. Meißner, Phys. Rev. D **90**, 034507 (2014).

[45] I. Tanihata, H. Hamagaki, O. Hashimoto, Y. Shida, N. Yoshikawa, K. Sugimoto, O. Yamakawa, T. Kobayashi, and N. Takahashi, Phys. Rev. Lett. **55**, 2676 (1985).

[46] J. Meng, H. Toki, S. Zhou, S. Zhang, W. Long, and L. Geng, Progress in Particle and Nuclear Physics **57**, 470 (2006).

[47] A. Bohr, Rev. Mod. Phys. **48**, 365 (1976).

[48] S. Altmann, Math. Proc. Cambridge **50**, 343 (1957).

[49] K. Rykhlinskaya and S. Fritzsche, Computer Physics Communications **174**, 903 (2006).